УДК 551.466.82

© *А. В. Кошелева*[*], *И. О. Ярощук*, *Ф. Ф. Храпченков*, *А. А. Пивоваров*, *А. Н. Самченко*, *А. Н. Швырев*, *Р. А. Коротченко*

Тихоокеанский океанологический институт им. В.И. Ильичева Дальневосточного отделения РАН, 690041, ул. Балтийская, 43, г. Владивосток, Россия
*E-mail: kosheleva@poi.dvo.ru

АПВЕЛЛИНГ НА УЗКОМ ШЕЛЬФЕ ЯПОНСКОГО МОРЯ В 2011 Г.

Статья поступила в редакцию 30.08.2020, после доработки 08.12.2020

На основе инструментальных и спутниковых наблюдений рассматриваются характерные особенности локального апвеллинга, наблюдавшегося в октябре 2011 г. в юго-западной части залива Петра Великого Японского моря. Кроме того, приведены результаты численного моделирования, выполнявшегося при помощи Regional Ocean Model System (ROMS) со свободной поверхностью. При вычислениях использовались метеорологические наблюдения за неоднородностями поля ветра и инструментальные измерения гидрологической структуры воды. Анализ данных натурных измерений и их сравнение с результатами моделирования развития апвеллинга выявили, что пространственный и временной масштаб явления определялся силой, продолжительностью и направлением воздействующего ветра. Неоднородность поля скорости ветра, тесно связанная с особенностями береговой орографии, приводит к усилению апвеллинга у некоторых частей побережья и формированию температурных фронтов и струй холодной воды, поперечных основному течению, идущему вдоль шельфа.

Ключевые слова: прибрежный апвеллинг, Японское море, спутниковые наблюдения, численное моделирование, ROMS, модель океана.

© *A. V. Kosheleva**, *I. O. Yaroshchuk*, *F. F. Khrapchenkov*, *A. A. Pivovarov*, *A. N. Samchenko*, *A. N. Shvyrev*, *R. A. Korotchenko*

V.I. Il`ichev Pacific Oceanological Institute, Far Eastern Branch of RAS, 690041, Baltiyskaya Str., 43, Vladivostok, Russia
*E-mail: kosheleva@poi.dvo.ru

UPWELLING ON THE NARROW SHELF OF THE SEA OF JAPAN IN 2011

Received 30.08.2020, in final form 08.12.2020

Characteristic features of a local upwelling observed in October, 2011 in the southwestern part of the Peter the Great Bay, the Sea of Japan, were studied using in situ and satellite observations. The paper presents as well the results of numeric simulation carried out with Regional Ocean Model System (ROMS) with a free surface. Meteorological observations of the wind field inhomogeneities as well as the results of in situ measurements of the seawater structure were used in the calculations. The analysis of in situ data and comparison with the simulation results of the upwelling development revealed that spatial and temporal scale of the phenomenon was determined by the force, the duration and the direction of wind. Inhomogeneity of the wind field over the Peter the Great Bay is closely associated with the peculiarities of coastal orography and leads to an upwelling intensification over some areas of the coast and to the creation of temperature fronts and cross-jets of cold water, transverse to the main current running along the shelf.

Key words: Coastal upwelling; Sea of Japan; satellite data; numerical modeling; ROMS; ocean model.

1. Introduction

A study of water exchange processes between the coastal shelf and the deep sea is one of the problems of the coastal oceanography. The upwelling development in the coastal area, with subsequent involvement of the displaced water masses into the vortex structures, moving along the continental slope, is one of the reasons of water exchange origin. Together with other factors, it leads to appearance of local areas of high biological productivity important for aquaculture and fisheries.

Ссылка для цитирования: *Кошелева А.В.*, *Ярощук И.О.*, *Храпченков Ф.Ф.*, *Пивоваров А.А.*, *Самченко А.Н.*, *Швырев А.Н.*, *Коротченко Р.А.* Апвеллинг на узком шельфе Японского моря в 2011 г. // Фундаментальная и прикладная гидрофизика. 2021. Т. 14, № 1. С. 31–42. doi: 10.7868/S2073667321010032

For citation: *Kosheleva A.V.*, *Yaroshchuk I.O.*, *Khrapchenkov F.F.*, *Pivovarov A.A.*, *Samchenko A.N.*, *Shvyrev A.N.*, *Korotchenko R.A.* Upwelling on the Narrow Shelf of the Sea of Japan in 2011. *Fundamentalnaya i Prikladnaya Gidrofizika*. 2021, 14, 1, 31–42. doi: 10.7868/S2073667321010032

The development of wind-induced upwelling in the Northern Hemisphere occurs under prolonged influence of wind: blowing southward along the eastern boundary of the ocean (sea) and northward along the western boundary of the ocean, with the subsequent upwelling of cold near-bottom water to the surface near the coast [1]. This coastal water circulation induced by wind has been an object for oceanographic studies since a long time [2–8]. In the Pacific region, regular wind-induced upwelling events were observed in the Sea of Okhotsk and in the Sea of Japan [9–11]. The upwelling phenomena were also observed and studied in detail using both satellite and in situ measurements in the southwestern part of the Sea of Japan near the coast of Korea [12], and in the South China Sea [13–17].

Using satellite imagery in the infrared range for several years, the areas of upwelling were noticed in the Peter the Great Bay and in the northwestern part of the Sea of Japan in summer and autumn [9, 10]. In the sea surface temperature (SST) fields, the cold water was observed along the northwestern coastline of the Sea of Japan. The water temperature distribution both in horizontal and vertical directions on the shelf is characterized by a significant temporal variability; the structural readjustment of the temperature field may occur within a few days. Cold areas are bounded by sharp thermal fronts. The upwelling of cold water to the surface layer in summer and autumn seasons is mainly wind-induced [9].

Cold waters near the northwestern coastline of the Sea of Japan and the system of thermal fronts associated with them are well detected in the satellite infrared images in summer and autumn months almost every year. In autumn, the cold water in coastal areas is observed regularly, up to the destruction of vertical stratification [18]. Wind nature of upwelling off the Primorye coast is caused by the monsoon variability of wind fields in different seasons [9, 10]. The upwelling off the southern Primorye coast may be caused by the southwestern and northwestern winds, and off the eastern and northeastern Primorye coast, — only by southwestern wind. The period from September to November is the most favorable for upwelling development in the south of Primorye coast. According to satellite data, most of the cases of the cold-water appearance off the eastern coast of Primorye occurs in October and only random upwelling events were observed in July — September [9, 10]. Wind field inhomogeneity over the Peter the Great Bay is associated with regional orographic peculiarities [19, 20],

However, the previous works used very few in situ observations. The water structure during upwelling was analyzed mainly using the data of several hydrological sections with large distances between stations. The dynamic characteristics of upwelling were estimated with empirical formulas. Previous studies [9, 10] on the Russian part of the Pacific coast include data of several hydrological sections and they make it possible to analyze the conditions of upwelling. The works devoted directly to upwelling phenomenon are mainly theoretical [10] and related to the analysis of satellite images [9].

To understand the process of upwelling of cold bottom water to the surface better, it is necessary to use a mathematical model containing parameters such as currents' speed, the velocity of the upwelling front movement, vertical speed in the upwelling areas, changes in salinity, etc. As the complete data set containing all of the above parameters did not exist, one of the goals of our work was to create an appropriate dataset to take into account the measured and simulated parameters.

This paper presents the results of observation of a local upwelling, which occurred in October, 2011 in the southwestern part of the Peter the Great Bay, as well as the numeric simulation of this event, and the obtained results are compared. The study was made on the basis of the analysis of satellite infrared imagery, meteorological observations, supplemented with Conductivity-Temperature-Depth (CTD) measurements. Long-term in situ measurements of the hydrological structure by means of thermostrings (vertical anchored thermode strings) were added to this complex of research and the authors found them to be very efficient.

The study was carried out for a narrow shelf region of 25–30 km, described in detail in [21], while the previous works on the upwelling in the Pacific region were done in the areas where the width of the shelf zone is hundreds of kilometers [8, 14, 17].

2. Data and Methods

In fig. 1, the region of interest is presented: the southwestern part of the Peter the Great Bay, with the Posyet Bay and adjacent waters. The site is rather small (about 600 km^2, where more than half of it is the Posyet Bay), but should be considered as representative, as it includes both the shallow water area and the beginning of the continental slope. The shelf width is 36 km from the 0 to 200 m depth. The bottom topography is characterized by relatively smooth deepening from 5 m/km up to 100 m isobath, then followed by more pronounced 20 m/km depth change for the range from 100 m to 200 m, with a further sharp depth increase of 210 m/km over the depths from 200 to 2000 m.

The Marine Experimental Station (MES) "Schultz Cape" of V.I. Il`ichev Pacific Oceanological Institute (POI) is situated in this area. Acoustical, oceanological, and geophysical studies are regularly carried out by the staff (and personally by the authors) in spring (mostly in May), summer, and autumn seasons. It made it possible to accumulate enough observation data over the period of time we were interested in.

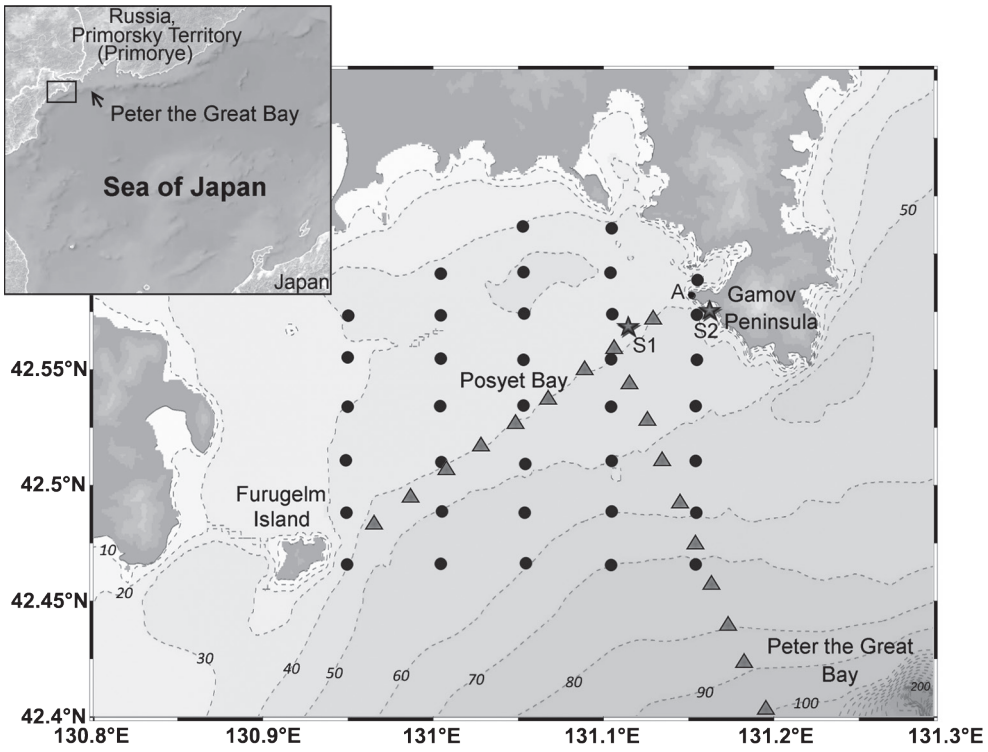

Fig. 1. The study area shown as the rectangle at the Sea of Japan map in the upper left corner and its detailed view. "A" is the "Aanderaa" meteorological station located at the Marine Experimental Station "Schultz Cape"; the stars show location of S1 and S2 thermostrings; circles are the CTD background survey stations; triangles are the points of the CTD sections.

The peculiarities of wind field at 70 m over the sea level were shown using wind speed observations at the meteorological station (MS) "Aanderaa" AWS2700 (letter "A" in fig. 1), located at the MES. The discreteness of the original data recording was about 30 s. We chose the data series from October 10 00:00 to October 23 00:00, 2011 and from October 10 00:00 to October 17 00:00, 2013. For visualization purposes, wind vectors are shown with a discreteness of 1 h.

The thermostrings were designed and constructed in POI for prolonged (over two weeks) temperature observations. These systems were described in detail in [22]. The thermostrings (S1 and S2 in fig. 1) were placed at depths of 42 and 19 m, at distances of 3 and 0.3 km off the coast, with the number of sensors 12 and 30, respectively. The vertical distance between the sensors at S1 string was 3 m, and at S2–0.5 m. The discreteness of the original data recording was 1 s for S1 and 20 s for S2. We used the data averaged to 1 min over the period from October 13 00:00 until October 23 00:00, 2011. S1 system operated until 15:30 on October 20, and then it was uninstalled. So, the available data set was accordingly shorter. The measurements on the S2 thermostring were carried out from August to the end of October, 2011. In October, 2013 the S1 thermostring was installed at the same place and we used its data registered from October 10 00:00 until October 17 00:00, 2013.

CTD profiling was another important source of in situ data used to assess the variability of water vertical structure (background survey and 3 hydrological sections). We used the RBR XR-620 instrument in our measurements. The procedure of data processing and correction of dynamic errors is described in [23]. The background survey was carried out from 11:00 until 20:00 on October 14 from the board of small research vessel "Malakhit" by CTD profiling at 36 stations (circles in fig. 1), one vertical profile at each station. In addition, two hydrological sections (triangles in fig. 1) were carried out along (from 13:30 until 15:30 on October 18 and from 10:00 until 11:40 on October 20) and across the isobaths (from 11:50 until 14:50 on October 15).

The infrared images made by the spectroradiometer MODIS of the "Aqua" satellite on October 16 at 17:19, October 17 at 04:25, and October 19 at 04:13 (GMT), 2011 were used as one of the main sources of data for the analysis and model verification. They were downloaded from [24] as SST distribution images in the Mercator projection with a resolution of 1.1 km. Later they are referred as made on October 17 at 04:19, on October 17 at 15:25, and on October 19 at 15:13 according to the local time (GMT+11:00) for easier comparison with in situ measurements and simulation results.

The Regional Ocean Model System (ROMS) was chosen to simulate the hydrophysical fields, as it was already used to study the upwelling events in other regions [25]. ROMS is a regional ocean model with a free surface based on the fundamental hydrodynamic equations. Stretched vertical coordinates (*S*-coordinates) are used mainly to increase the vertical resolution of the model on the shelf and for the coastal areas with open side borders (like our study region). Conversion of current velocity fields in the layers from terrain-following *S*-coordinates used in ROMS to the commonly used Cartesian *Z*-coordinates was carried out with the formulas of [26]. It should be note that similar approach was successfully used for numerical modeling of circulation in the entire Peter the Great Bay and adjacent areas [cf. 27].

Our model was running on the period of October 10–21, 2011. The simulated area is the same that the area of in situ measurements shown in fig. 1. The northern and western boundaries of the modelled region are closed and correspond to the coastline. The model has a horizontal resolution of 100 meters with 20 vertical layers, and the time step is 2 s. The data of the background hydrological survey carried out on October 14, 2011 were used as initial conditions for simulation. Data from 36 points of the background survey were interpolated by bicubic interpolation method to use in computational grid of the model as initial data on temperature and salinity. As the current velocity initial data and the boundary values of salinity, temperature current velocity, the results of ROMS climate modeling in the Peter the Great Bay [27] for that season were used. Atmospheric forcing data were taken from the actual observations at the MS "Aanderaa" for October 10–21, 2011.

3. Results

Previous studies [19, 20] revealed wind field inhomogeneity caused by regional orographic peculiarities of the southwestern Primorye. In the inner harbors of the Peter the Great Bay and adjacent areas, a significant wind increase occurred. We have compared wind measurements at MS "Aanderaa" located on the eastern coast of the Posyet Bay with measurements at MS "Posyet" located on its western coast. Over the same period of time, there was a significant difference both in direction and in speed of wind at these stations: e. g., the wind speed at the northeastern coast ("Aanderaa") was almost twice higher than that at the western coast ("Posyet") on October 16, 2011 [28].

The meteorological data show that strong (9–20 m/s) northwestern wind started on October 16 and continued until the evening of October 19, 2011, then the wind speed decreased and its direction became unstable (fig. 2, *a*; see Inset).

Available satellite images of SST for October 17 and 19, 2011 (fig. 3, *a* and *b*; see Inset) show the spread of a zone with low SST along the coast, concurring with strengthening of western and northwestern winds. Unfortunately, there are many clouds, especially in fig. 3, *b*. But the thermal fronts between warm and cold water in the coastal area are well seen. Cold water jets stretching for dozens of kilometers in the southern direction are clearly visible in the consecutive images of October 17 and 19 (fig. 3, *b* and *c*). As we can see in fig. 3, *b*, cold water is noticed at distances of 10–50 km from the coast, in accordance with the bottom topography, and along the coastline it extends for about a hundred kilometers. We can see in fig. 3, *c* that cold waters were partially carried eastward from Posyet Bay and then to the south by vortex structures near the shelf break.

In situ data obtained with the S1 (fig. 2, *b*) and S2 (fig. 2, *c*) thermostrings allowed us to observe the development of extended upwelling in the early second half of October. Moreover, since the S2 system worked from August to the end of October, 2011, we could trace the change in the vertical distribution of water temperature off the coast also in previous period. Decrease of the temperature in the coastal area in September-October, 2011, was happening in stages, and was mainly wind-induced. The first "step" was a temperature decrease in the surface layer from 23 to 20 °C, with further gradual decrease of water temperature to 19–18 °C, that took place in the middle of September. The next step is a water temperature decrease from 18.5 to 15 °C, when on some days the water temperature in the surface layer decreased to 13 °C for a few hours, occurred on September 30. Later, up to October 16, water temperature decreased gradually, varying from 15 to 12 °C (fig. 4; see Inset). Northwestern wind with increase of up to 15–20 m/s on October 16–17 (fig. 2, *a*) led to development of the most extensive upwelling in the end of the second decade of October off the coast of entire Primorye. In the study area the water temperature in the near-surface layer in coastal area decreased from 12 to 3–5 °C (fig. 4, *a*), while in the central part of the Posyet Bay it was about 5 °C (fig. 4, *b*).

In the beginning of September, the thermocline was located at the depth from 7–10 m to 20–30 m; on October 14, it became narrower and was located at the depth from 10 to 15–20 m. During the upwelling on October 18 the thermocline in the seaward part of the Posyet Bay moved down to the depths of 20–25 m, and came out to the sea surface at the distance of 2–3 km from the shore at the Gamov Peninsula forming a thermal front. At that, the water temperature in the upper layer decreased from over 13 to 8 °C in the middle part of the Posyet Bay and to 5–6 °C in the coastal area. In the bottom layer the water temperature decreased from 3.5 °C to less than 2.4 °C, which indicates the movement of colder water from the depths of over 100 m directly to the coast (fig. 5; see Inset).

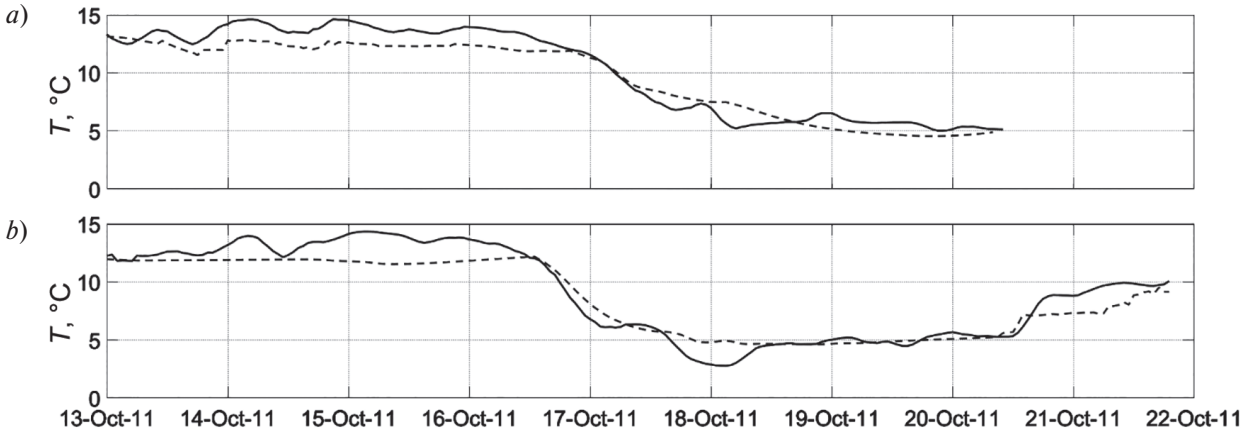

Fig. 6. Time variability of the water temperature averaged to 1 h according to the upper sensors (at the depth of 3 m) of S1 (*a*) and S2 (*b*) thermostrings. Dashed lines — ROMS simulated temperature for the surface layer in the appropriate points.

Data of observations from the thermostrings, located at different distances from the coast at the depths of 19 and 42 m, allowed us to observe the upwelling development in the coastal area. In the morning of October, 16 the surface homogeneous layer was observed down to the depth of 5 m with the temperature over 13 °C, the thermocline was located at the depth of 7–20 m (isotherms were horizontal), the 4 °C isotherm was located at the depth of 25 m and minimum water temperature near the bottom was about 3.5 °C. In less than a day, at 2:00 on October 17, the water temperature decreased to 6.5–7 °C near the coast, and at the distance of 3 km off the coast it decreased to 8–9 °C. The isotherms have an incline from the coast towards the sea, and in the bottom layer the water with temperature of less than 3 °C came up. This indicates that at the sea surface the outflow of warmer waters to the open sea had occurred, and in their place the upwelling of colder water began, which continued for a day under the influence of strong west-north-western wind. The result was that the upwelling had reached its maximum development by 02:00 of October 18, the water with temperature of 2.5–3 °C came out to the sea surface near the shore and the 4 °C isotherm moved up from the depth of 15 m to the surface at about 1.5 km from the coast (fig. 5, *c*). In the coastal area from 18:00 on October 17 and during following 10 hours the minimum difference in near-bottom and near-surface water temperature was observed (less than 1 °C), meanwhile, the water temperature at the bottom decreased to 2.2 °C. The maximum speed of water temperature variation near the sea surface reached 6 °C per hour (1 °C per 10 min), and in the average — 0.83 °C per hour (5 °C per 6 hours).

The wind decrease (down to 6.2 m/s) in the second half of October 18 led to the fact that by 22:00 of the same day in the coastal area temperature increased to 5 °C, and 4 °C isotherm had lowered to the depth of 15–20 m. Subsequently the water temperature in the surface layer became even higher and on October 21 it was already 9–10 °C.

The upwelling development can be estimated according to the data of the upper thermostring sensors located at the depth of 3 m from the sea surface and at 3.0 (fig. 6, *a*) and 0.3 (fig. 6, *b*) km distance from the coast.

The maximum water temperature variations were observed in the coastal area with the minimum water temperature of 2.7 °C, which was observed during 10 hours. Decrease of the water temperature at 3 km off the coast began 5–6 hours later and the minimum temperature values were registered 4 hours later than those near the coastline.

The average speed of the upper layer warm waters displacement offshore and cold bottom waters onshore was 0.15–0.20 m/s.

4. Simulation

The upwelling was observed from October 17 till October 19, 2011, therefore, the model allowed to trace variations of the hydrodynamic characteristics of the water area in the specified period of time. The calculated map of currents in the study area as of October 16, 2011 is presented in fig. 7.

However, the map of surface currents changed after the wind strengthening. The map of surface currents for October 18, 2011 is shown in fig. 8, and corresponds to the peak of the upwelling phenomenon development.

As we can see in the map, the surface currents changed completely: the prevailing current direction changed from the northeast to the south, and the maximum speed of the surface current increased by 20–25 cm/s; the removal of water masses occurred. At the same time, the bottom currents (fig. 9) contained a compensation component and their velocities were significantly lower than those in the surface layer (fig. 8).

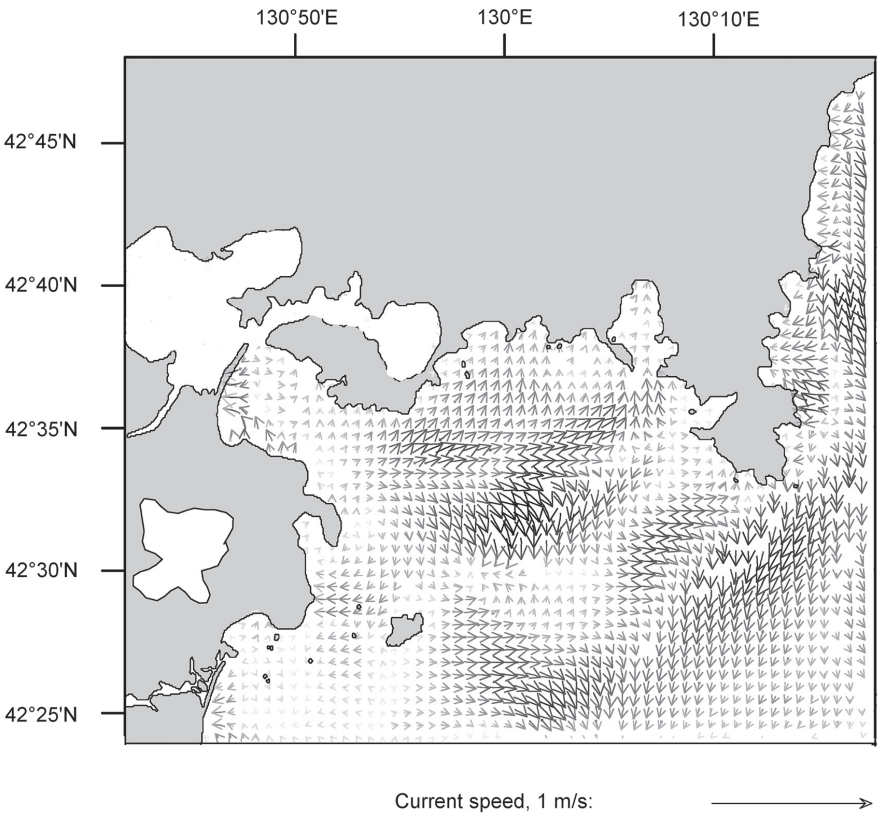

Fig. 7. Simulated surface currents in the study area as of October 16, 2011 before the upwelling event.

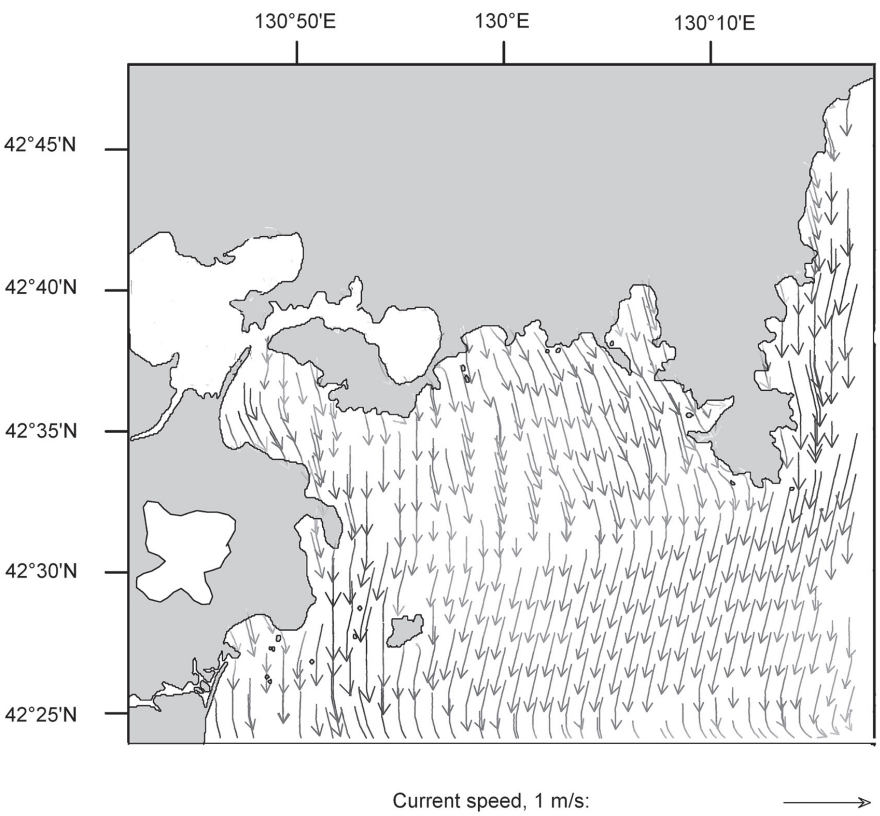

Fig. 8. Simulated surface currents in the study area at the peak of upwelling development on October 18, 2011.

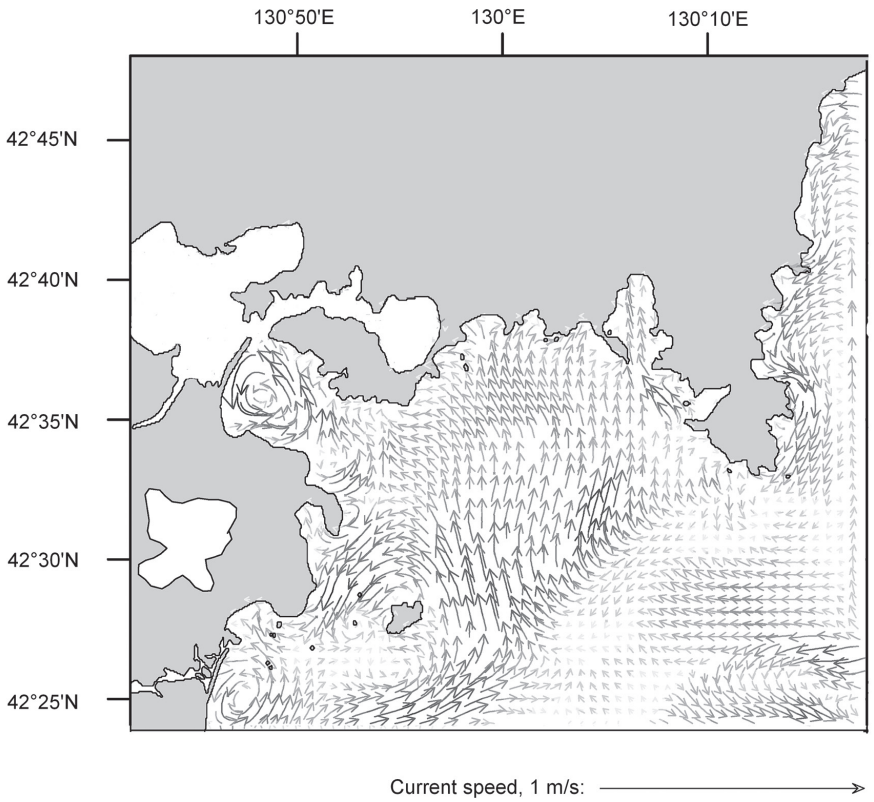

Fig. 9. Simulated near-bottom currents in the study area at the peak of upwelling development on October 18, 2011.

The prevailing current direction in the bottom layer is the northward, this fact corresponds to the picture of currents under the upwelling influence. At the same time, in the intermediate layer the currents change direction abruptly. It corresponds to the movement of deep cold waters coming from the shelf break into the Posyet Bay in the bottom layer; and warm waters moving offshore through the surface in accordance with the classical picture of upwelling.

The simulated temperature fields were checked against satellite observations and data of the thermostrings located in the Posyet Bay during the upwelling phenomenon. The comparison of the simulated (dashed lines in fig. 6, *a* and *b*) with the observed data (solid lines in the same figures) was carried out. The mean temperature difference between the upper thermostring sensors measurements and the surface layer temperature in the model does not exceed 1 °C. The difference in time of the occurrence and disappearance of upwelling phenomenon in the model in comparison with the real data sets is less than two hours. The correlation coefficient between in situ and simulated temperature time series for the period of October 10–21, 2011 is equal to 0.89.

Vertical velocities in the model were determined by integrating the grid continuity equation taking into account the *S*-surface curvature. In accordance with the equations of [29] the vertical dynamics of water structure was evaluated in *Z*-coordinate system, the results for the peak of upwelling development are shown in table 1. We should note that in case of vertical velocity, in the open part of the Posyet Bay the velocities decrease in modulus to 0.2–0.4 mm/s and can take the opposite directions.

SST maps simulated by ROMS for the beginning, development and the peak of upwelling are shown in fig. 10, *a*, *b*, and *c*, respectively; and compared with appropriate satellite images (fig. 3, *a*, *b*).

Table 1

Vertical and horizontal current velocities in different layers at the peak of upwelling development on October 18, 2011

Layer depth, m	Vertical velocity (in the areas of active upwelling near the coast), mm/s	Horizontal velocity, cm/s
0–20	2.2	≤ 45
20–60	1.6–1.8	≤ 35
60–100	0.5–1.4	≤ 18

At the peak of the upwelling development, it was cloudy over the southern part of the Peter the Great Bay. Therefore, fig. 3, *c* and fig. 10, *c* are not synchronize in time, but the real temperature pattern as a whole can be considered as corresponding to the model in fig. 10, *c*. The prevailing SST was from 5 to 10 °C, decreasing to 3 °C near the coast.

5. Discussion

As we know, the basic mechanisms of coastal upwelling are connected with wind influence, bottom topography and tidal processes [1].

The monsoon character of the atmospheric circulation and the considerable synoptic wind variability lead to different-scale variations of stratification and current system in the bay and the adjacent part of the deep sea [18]. During the transition from summer to winter monsoon, northwestern wind becomes prevailing [20]; in this area, it leaves the coast on the left and leads to recession of the upper mixed water layer off the coast, appearance of the pressure gradient and transfer of cold bottom water to the shore with its appearance at the sea surface.

Model simulation showed that when the wind speed is more than 15 m/s, it can cause the upwelling development. Weaker wind, in combination with other factors, can also induce a short-term upwelling. In October, similar phenomena are observed in the study area almost every year [9]. Fig. 11 shows manifestations of local upwelling events in 2013: a more pronounced one on October 12–13, 2013, and less pronounced — on October 15, 2013 (see Inset).

The previously revealed wind field inhomogeneity in the Peter the Great Bay [19, 20] leads to significant wind increase over some parts of the Bay and, in consequence, to upwelling intensification in some coastal areas and to the creation of temperature fronts and jets of cold water transverse to the main current running along the shelf.

Along with the traditional mechanisms for the occurrence of stepwise wave fronts formed in downward currents under the wind influence, there is also a less studied mechanism for the generation of internal bores when high-amplitude waves enter the shelf zone.

Studies of internal waves in the coastal zone [30–32] revealed a characteristic set of wave configurations determined by substantially nonlinear processes. Among such configurations, internal bore is an example of such nonlinear process: it is a result of an abrupt change in the depth of the pycnocline. These processes can be observed in September-October when conducting in situ measurements in the study area [31]. This wave is an internal wave pushing the pycnocline up and down [30]. Along the front of the internal bore, intense internal waves are also generated. The process of disintegration of a smooth internal bore and its transformation into a train of solitary high-amplitude waves when entering the shelf zone is studied both experimentally and theoretically [21, 22]. Nonlinear internal waves are able to transport energy over long distances efficiently and are therefore likely to be an important mechanism for transporting and distributing nutrients, pollutants, sediment, planktonic organisms and other suspended substances on the shelf of coastal areas. The presence of a near surface pycnocline probably provides a significant energy transfer over the shelf when strong baroclinic internal tides spread along the edge of the bay shelf, while the position of the thermocline changes vertically by 10 m [32]. However, this does not lead to the appearance of cold water at the surface near the coast.

In early autumn, the pycnocline in our region on the shelf can move down to the bottom due to the increase in thickness of surface homogeneous layer up to 40–50 m, but its own thickness at the same time does not exceed 15–25 m [30].

Analysis of satellite imagery revealed the presence of anticyclonic vortex structures moving along the continental slope of the Peter the Great Bay to the southwest, their amplification and weakening during the meteorological synoptic period, as well as the presence of cyclonic vortices with subsynoptic scale (up to 10 km) [33]. The appearance of these synoptic vortices is caused by hydrodynamic instability over the narrow shelf and continental slope of the bay, where their lifetime does not exceed 20 days.

Horizontal scale of anticyclonic vortices moving and stationing on the shelf of the bay roughly corresponds to the Rossby radius of deformation, which increases from the beginning of warm season (May-June) through its middle (August) to the end (September-October) from 15 to 35–40 km, which is accompanied by the pycnocline thickness increase [18, 33]. The cyclonic vortices are also formed of both synoptic and subsynoptic scales directly on the shelf. In September-November and in the winter season, relatively warm jet flows and vortices are formed in the southwestern border area of the bay and the adjacent part of the deep sea bordering on the northwestern subarctic front.

Such vortex structures in the upper mixed sea layer and the currents induced at the same time may contribute both to the transfer of cold bottom water to the coast, and to capture and remove off the coast the cold water appeared on the surface as a result of upwelling. It is accompanied by the creation of cold jets stretching off the coast for dozens of kilometers and clearly visible in satellite images of our area (fig. 3, *c*).

An advection time, which is a time of cold water upwelling from the deep sea to the surface in coastal area, in this case (October 2011) is about 12 hours according both to observation data and Peter the Great Bay numerical sim-

ulation. At the same time, the duration of wind of appropriate direction and force of up to 10 m/s is up to 24 hours. With further wind increase up to 15–20 m/s in 12 hours the surface temperature near the coast reduced by another 3 degrees, i. e. to the minimum values. Total time of upwelling-favorable wind was 2.5 days. Thus, an "upwelling age" [34], in our case was equal to 5 days, which means that the coastal upwelling was well-developed, and strong thermal fronts were formed with significant horizontal gradients of water temperature observed in satellite images

6. Conclusions

Our research showed that influence of the northeastern wind with a speed of 15–20 m/s lasting for two days led to the development of upwelling over the whole study area. It became evident due to the warm water offshore outflow in approximately 20–30 meter upper layer with speed of 40–45 cm/s and compensating inflow of cold water in the bottom layer of the depth from 40 to 90 m with a typical speed of about 18 cm/s, which is confirmed by the model. Pronounced coastal upwelling was observed along the coast of the Gamov peninsula, in the northern and western harbors of the area. In these places the vertical upwelling speed reached 2 mm/s.

The vertical circulation typical for upwelling in the bays of the study area began only after 10–11 hours after a strong northwestern wind effect; before the upwelling, there was an insignificant wind-induced recession within the range 3–5 °C.

After the end of wind influence on the hydrodynamic system, it remained in a stable equilibrium state without changing its circulation. In the end of the second day, the restoring process of the previous currents structure started. At the same time, fluctuations in temperature and speed of currents were induced in the bottom layer with a period from inertial, 17 hours, to daily, attenuating during 5 days after the upwelling completion.

To sum up, the phenomenon of wind-induced upwelling on the narrow shelf of the Sea of Japan has been studied in detail for the first time using thermostring measurements (long-term observations in 2 fixed points), a background CTD survey (the spatial distribution of hydrological characteristics), detailed meteorological data, satellite imagery and numeric simulation based on experimental data (ROMS).

However, it is necessary to take into account the other factors affecting the displacement of a cold from the continental slope to the coast, such as vortex structures or internal waves. The annual upwelling in the Posyet Bay in October is also associated with the restructuring of the atmospheric circulation (transition to the winter monsoon). Since such repetitive events have a significant impact on the development of aquaculture and fishing in the coastal part of the Bay, they deserve attention and study.

7. Acknowledgements

The authors would like to thank Sergey Smirnov and Igor Oleynikov for their help in preparing this paper.

8. Funding

The investigation was partly supported by the State Task for the POI FEB RAS (state registration No. AAAA-A20–120021990003–3).

Литература

1. *Боуден К.* Физическая океанография прибрежных вод / Пер. с англ. М.: Мир, 1988. 324 с.
2. *Preller R., O'Brien J.J.* The Influence of Bottom Topography on Upwelling off Peru // J. Phys. Oceanogr. 1980. V. 10, N9. P. 1377–1398. doi: 10.1175/1520–0485(1980)010<1377: TIOBTO>2.0.CO;2
3. *Zaytsev O., Cervantes-Duarte R., Montante O., Gallegos-Garcia A.* Coastal upwelling activity on the Pacific Shelf of the Baja California Peninsula // J. Oceanogr. 2003. V. 59, N 4. P. 489–502. doi: 10.1023/A:1025544700632
4. *Perlin N., Skyllingstadet E., Samelson R., Barbour P.* Numerical Simulation of Air-Sea Coupling during Coastal Upwelling // J. Phys. Oceanogr 2007. V. 37, N 8. P. 2081–2093. doi: 10.1175/JPO3104.1
5. *Dippner J.W., Nguyen K.V., Hein H., Ohde T., Loick N.* Monsoon-induced upwelling off the Vietnamese coast // Ocean. Dyn. 2007. V. 57, N 1. P. 46–62.doi: 10.1007/s10236–006–0091–0
6. *Rao A.D., Joshi M., Ravichandran M.* Oceanic upwelling and downwelling processes in waters off the west coast of India // Ocean. Dyn. 2008. V. 58, N 3/4. P. 213–226. doi: 10.1007/s10236–008–0147–4
7. *Chen Z., Yan X.-H., Jiang Y., Jiang L., Jo Y.-H.* A study of cross-shore maximum upwelling intensity along the Northwest Africa coast // J. Oceanogr. 2013. V. 69, N 4. P. 443–450. doi: 10.1007/s10872–013–0185–5
8. *Daryabor F., Samah A.A., Ooi S.H.* Dynamical structure of the sea off the east coast of Peninsular Malaysia // Ocean. Dyn. 2015. V. 65, N 1. P. 93–106. doi: 10.1007/s10236–014–0787–5

9. *Жабин И.А.*, *Грамм-Осипова О.Л.*, *Юрасов Г.И.* Ветровой апвеллинг у северо-западного побережья Японского моря // Метеорология и гидрология. 1993. № 10. С. 82–86.
10. *Юрасов Г.И.*, *Вилянская Е.А.* Характеристики апвеллинга в заливе Петра Великого в осенне-зимний сезон 1999–2000 гг. // Метеорология и гидрология. 2010. № 10. С. 54–63.
11. *Lu L.-F.*, *Onishi R.*, *Takahashi K.* The effect of wind on long-term summer water temperature trends in Tokyo Bay, Japan // Ocean. Dyn. 2015. V. 65, N 6. P. 919–930. doi: 10.1007/s10236–015–0848–4
12. *Park K.-A.*, *Kim K.-R.* Unprecedented coastal upwelling in the East/Japan Sea and linkage to long-term large-scale variations // Geophys. Res. Lett. 2010. V. 37, N 9. L09603. doi: 10.1029/2009GL042231
13. *Su J.*, *Wang J.*, *Pohlmann T.*, *Xu D.* The influence of meteorological variation on the upwelling system off eastern Hainan during summer 2007–2008 // Ocean Dyn. 2011. V. 61, N 6. P. 717–730. doi: 10.1007/s10236–011–0404–9
14. *Shu Y.*, *Wang D.*, *Zhu J.*, *Peng S.* The 4-D structure of upwelling and Pearl River plume in the northern South China Sea during summer 2008 revealed by a data assimilation model // Ocean Model. 2011. V. 36, N 3–4. P. 228–241. doi: 10.1016/j.ocemod.2011.01.002
15. *Jiang Y.*, *Chai F.*, *Wan Z.*, *Zhang X.*, *Hong H.* Characteristics and mechanisms of the Upwelling in the southern Taiwan Strait: a three-dimensional numerical model study // J. Oceanogr. 2011. V. 67, N 6. P. 699–708. doi: 10.1007/s10872–011–0080-x
16. *Wang D.*, *Shu Y.* et. al. Relative contributions of local wind and topography to the coastal upwelling in the northern South China Sea // J. Geophys. Res. 2014. V. 119, N 4. P. 2550–2567. doi: 10.1002/2013JC009172
17. *Lin P.*, *Hu J.*, *Zheng Q.*, *Sun Z.*, *Zhu J.* Observation of summertime upwelling off the eastern and northeastern coasts of Hainan Island, China // Ocean. Dyn. 2016. V. 66, N 3. P. 387–399. doi: 10.1007/s10236–016–0934–2
18. *Пономарев В.И.*, *Файман П.А.*, *Дубина В.А.*, *Ладыченко С.Ю.*, *Лобанов В.Б.* Синоптическая вихревая динамика над северо-западным материковым склоном и шельфом Японского моря (моделирование и результаты дистанционных наблюдений) // Современные проблемы дистанционного зондирования Земли из космоса. 2011. Т. 8, № 2. С. 100–104.
19. *Дубина В.А.*, *Митник Л.М.*, *Катин И.О.* Особенности циркуляции вод залива Петра Великого на основе спутниковых мультисенсорных данных // Современное состояние и тенденции изменения природной среды залива Петра Великого Японского моря / Под ред. Акуличева В.А. М.: ГЕОС, 2008. С. 82–96.
20. *Полякова А.М.* Характеристика процессов волнения в заливе Петра Великого // Современное состояние и тенденции изменения природной среды залива Петра Великого Японского моря / Под ред. Акуличева В.А. М.: ГЕОС, 2008. С. 110–133.
21. *Коротченко Р.А.*, *Самченко А.Н.*, *Ярощук И.О.* Пространственно-временной анализ геоморфологии дна залива Петра Великого (Японское море) // Океанология. 2014. Т. 54, № 4. С. 538–545. doi: 10.7868/S0030157414030046
22. *Леонтьев А.П.*, *Ярощук И.О.*, *Смирнов С.В.*, *Кошелева А.В.*, *Пивоваров А.А.*, *Самченко А.Н.*, *Швырев А.Н.* Пространственно-распределенный измерительный комплекс для мониторинга гидрофизическихпроцессов на океаническом шельфе // Приборы и техника эксперимента. 2017. № 1. С. 128–135. doi: 10.7868/S0032816216060227
23. *Kosheleva A.V.*, *Lazaryuk A. Yu.*, *Yaroshchuk I.O.* Estimation of acoustic and oceanological seawater characteristics by temperature measurements in the Sea of Japan shelf zone // Proc. Mtgs. Acoust. 2015. V. 24, 005001. doi: 10.1121/2.0000109
24. Центр коллективного пользования Регионального Спутникового Мониторинга Окружающей среды ДВО РАН. http://www.satellite.dvo.ru (дата обращения: 15.08.2020).
25. *Lorenzo E.D.*, *Moore A.M.*, *Arango H.G.* et. al. Weak and strong constraint data assimilation in the inverse Regional Ocean Modeling System (ROMS): Development and application for a baroclinic coastal upwelling system // Ocean. Model. 2007. V. 16, N 3–4. P. 160–187. doi: 10.1016/j.ocemod.2006.08.002
26. *Song Y.*, *Haidvogel D.B.* A semi-implicit ocean circulation model using a generalized topography-following coordinate system // J. Comp. Phys. 1994. V. 115, N 1. P. 228–244. doi: 10.1006/jcph.1994.1189
27. *Олейников И.С.*, *Юрасов Г.И.*, *Ищенко М.А.* Опыт применения системы численного моделирования ROMS для исследования гидродинамических процессов в заливе Петра Великого // Известия ТИНРО. 2011. Т. 166. С. 275–282.
28. Метеоцентр. Погода в Посьете. URL: http://meteocenter.net/31969_fact.html (дата обращения: 30.11.2011).
29. *Shchepetkin A.F.*, *McWilliams J.C.* A Method for Computing Horizontal Pressure-Gradient Force in an Oceanic Model with a Non-Aligned Vertical Coordinate // J. Geophys. Res. 2003. V. 108, C3. P. 3090. doi: 10.1029/2001JC001047
30. *Ляпидевский В.Ю.*, *Новотрясов В.В.*, *Храпченков Ф.Ф.*, *Ярощук И.О.* Внутренний волновой бор в шельфовой зоне моря // Прикладная механика и техническая физика. Т. 58, № 5. С. 60–71. doi: 10.15372/PMTF20170506
31. *Samchenko A.N.*, *Yaroshchuk I.O.*, *Kosheleva A.V.* Internal gravity waves in the coastal zone of the Sea of Japan according to the natural observations // Reg. Stud. Mar. Sci. 2018. N 18. P. 156–160. doi: 10.1016/j.rsma.2018.02.004
32. *Ярощук И.О.*, *Леонтьев А.П.*, *Кошелева А.В.*, *Пивоваров А.А.*, *Самченко А.Н.*, *Степанов Д.В.*, *Швырев А.Н.* Об интенсивных внутренних волнах в прибрежной зоне залива Петра Великого (Японское море) // Метеорология и гидрология. 2016. № 9. С. 55–62.

33. *Пранц С.В.*, *Пономарев В.И.*, *Будянский М.В.*, *Улейский М.Ю.*, *Файман П.А.* Лагранжев анализ перемешивания и переноса вод в морских заливах // Известия Российской академии наук. Физика атмосферы и океана. 2013. Т. 49, № 1. С. 91–106. doi: 10.7868/S0002351513010082

34. *Jiang L.*, *Breaker L.C.*, *Yan X.-H.* Upwelling age: an indicator of local tendency for coastal upwelling // J. Oceanogr. 2012. V. 68, N 2. P. 337–344. doi: 10.1007/s10872–011–0096–2

References

1. *Bowden K.F.* Physical oceanography of coastal waters. *Chichester*, *Ellis Horwood Ltd*., 1983, 302 p.

2. *Preller R.*, *O'Brien J.J.* The Influence of Bottom Topography on Upwelling off Peru. *J. Phys. Oceanogr.* 1980, 10, 9, 1377–1398. doi: 10.1175/1520–0485(1980)010<1377: TIOBTO>2.0.CO;2

3. *Zaytsev O.*, *Cervantes-Duarte R.*, *Montante O.*, *Gallegos-Garcia A.* Coastal Upwelling Activity on the Pacific Shelf of the Baja California Peninsula. *J. Oceanogr.* 2003, 59, 4, 489–502. doi: 10.1023/A:1025544700632

4. *Perlin N.*, *Skyllingstadet E.*, *Samelson R.*, *Barbour P.* Numerical Simulation of Air-Sea Coupling during Coastal Upwelling. *J. Phys. Oceanogr.* 2007, 37, 8, 2081–2093. doi: 10.1175/JPO3104.1

5. *Dippner J.W.*, *Nguyen K.V.*, *Hein H.*, *Ohde T.*, *Loick N.* Monsoon-induced upwelling off the Vietnamese coast. *Ocean. Dyn*. 2007, 57, 1, 46–62. doi: 10.1007/s10236–006–0091–0

6. *Rao A.D.*, *Joshi M.*, *Ravichandran M.* Oceanic upwelling and downwelling processes in waters off the west coast of India. *Ocean. Dyn*. 2008, 58, 213–226. doi: 10.1007/s10236–008–0147–4

7. *Chen Z.*, *Yan X.-H.*, *Jiang Y.*, *Jiang L.*, *Jo Y.-H.* A study of cross-shore maximum upwelling intensity along the Northwest Africa coast. *J. Oceanogr.* 2013, 69, 4, 443–450. doi: 10.1007/s10872–013–0185–5

8. *Daryabor F.*, *Samah A.A.*, *Ooi S.H.* Dynamical structure of the sea off the east coast of Peninsular Malaysia. *Ocean. Dyn*. 2015, 65, 1, 93–106. doi: 10.1007/s10236–014–0787–5

9. *Zhabin I.A.*, *Gramm-Osipova O.L.*, *Yurasov G.I.* Wind upwelling near the Sea of Japan northwest coast. *Meteorol. Gidrol.* 1993, 10, 82–86 (in Russian).

10. *Yurasov G.I.*, *Vilyanskaya E.A.* Upwelling characteristics in the Peter the Great Bay in Fall-Winter Season of 1999–2000. *Russ. Meteorol. Hydrol.* 2010, 35, 687–694. doi: 10.3103/S1068373910100067

11. *Lu L.-F.*, *Onishi R.*, *Takahashi K.* The effect of wind on long-term summer water temperature trends in Tokyo Bay, Japan. *Ocean Dyn*. 2015, 65, 6, 919–930. doi: 10.1007/s10236–015–0848–4.

12. *Park K.-A.*, *Kim K.-R.* Unprecedented coastal upwelling in the East/Japan Sea and linkage to long-term large-scale variations. *Geophys. Res. Lett*. 2010, 37, 9, L09603. doi: 10.1029/2009GL042231

13. *Su J.*, *Wang J.*, *Pohlmann T.*, *Xu D.* The influence of meteorological variation on the upwelling system off eastern Hainan during summer 2007–2008. *Ocean Dyn*. 2011, 61, 6, 717–730. doi: 10.1007/s10236–011–0404–9

14. *Shu Y.*, *Wang D.*, *Zhu J.*, *Peng S.* The 4-D structure of upwelling and Pearl River plume in the northern South China Sea during summer 2008 revealed by a data assimilation model. *Ocean Model*. 2011, 36, 3–4, 228–241. doi: 10.1016/j.ocemod.2011.01.002

15. *Jiang Y.*, *Chai F.*, *Wan Z.*, *Zhang X.*, *Hong H.* Characteristics and mechanisms of the Upwelling in the southern Taiwan Strait: a three-dimensional numerical model study. *J. Oceanogr.* 2011, 67, 6, 699–708. doi: 10.1007/s10872–011–0080-x

16. *Wang D.*, *Shu Y.* et. al. Relative contributions of local wind and topography to the coastal upwelling in the northern South China Sea. *J. Geophys. Res*. 2014, 119, 4, 2550–2567. doi: 10.1002/2013JC009172

17. *Lin P.*, *Hu J.*, *Zheng Q.*, *Sun Z.*, *Zhu J.* Observation of summertime upwelling off the eastern and northeastern coasts of Hainan Island, China. *Ocean Dyn*. 2016, 66, 3, 387–399. doi: 10.1007/s10236–016–0934–2

18. *Ponomarev V.I.*, *Fyman P.A.*, *Dubina V.F.*, *Ladychenko S.Y.*, *Lobanov V.B.* Mesoscale eddy dynamic over northwest Japan Sea continental slope and shelf (simulation and remote sensing results). *Sovr. Probl. DZZ Kosm.* 2011, 8(2), 100–104 (in Russian).

19. *Dubina V.A.*, *Mitnik L.M.*, *Katin I.O.* Features of water circulation in the Peter-the-Great Bay revealed by satellite multisensor data. Existing environmental condition and tendencies of its change in the Peter-the-Great Bay, the Sea of Japan / Ed. *Akulichev V.A. M.*, *GEOS*, 2008, 82–96 (in Russian).

20. *Polyakova A.M.* Characteristics of the wave processes in the Peter-the-Great Bay // Existing environmental condition and tendencies of its change in the Peter-the-Great Bay, the Sea of Japan / Ed. *Akulichev V.A.* M.: GEOS, 2008. P. 110–133 (in Russian).

21. *Korotchenko R.A.*, *Samchenko A.N.*, *Yaroshchuk I.O.* The spatiotemporal analysis of the bottom geomorphology in Peter the Great Bay of the Sea of Japan. *Oceanology*. 2014, 54, 4, 497–504. doi: 10.1134/S0001437014030047

22. *Leontyev A.P.*, *Yaroshchuk I.O.*, *Smirmov S.V.*, *Kosheleva A.V.*, *Pivovarov A.A., Samchenko A.N.*, *Shvyrev A.N.* A spatially distributed measuring complex for monitoring hydrophysical processes on the ocean shelf. *Instrum. Exp. Tech*. 2017, 60, 1, 130–136. doi: 10.1134/S0020441216060191

23. *Kosheleva A.V.*, *Lazaryuk A. Yu.*, *Yaroshchuk I.O.* Estimation of acoustic and oceanological seawater characteristics by temperature measurements in the Sea of Japan shelf zone. *Proc. Mtgs. Acoust.* 2015, 24, 005001. doi: 10.1121/2.0000109
24. Center for Regional Satellite Monitoring of Environment, Far Eastern Branch of Russian Academy of Sciences. URL: http://www.satellite.dvo.ru (date of access: 15.08.20).
25. *Lorenzo E.D.*, *Moore A.M.*, *Arango H.G.* et. al. Weak and strong constraint data assimilation in the inverse Regional Ocean Modeling System (ROMS): Development and application for a baroclinic coastal upwelling system. *Ocean Model.* 2007, 16, 3–4, 160–187. doi: 10.1016/j.ocemod.2006.08.002
26. *Song Y., Haidvogel D.B.* A semi-implicit ocean circulation model using a generalized topography-following coordinate system. *J. Comp. Phys.* 1994, 115, 1, 228–244. doi: 10.1006/jcph.1994.1189
27. *Oleynikov I.S.*, *Yurasov G.I.*, *Ishchenko M.A.* ROMS experience for investigation the processes in Peter the Great Bay. *Izv. TINRO.* 2011, 166, 275–282 (in Russian).
28. Meteocenter. Weather in Posyet. URL: http://meteocenter.net/31969_fact.html (date of access: 30.11.11).
29. *Shchepetkin A.F.*, *McWilliams J.C.* A Method for Computing Horizontal Pressure-Gradient Force in an oceanic model with a non-aligned vertical coordinate. *J. Geophys. Res.* 2003, 108, C3, 3090. doi: 10.1029/2001JC001047
30. *Liapidevskii V.Y.*, *Novotryasov V.V.*, *Khrapchenkov F.F.*, *Yaroshchuk I.O.* Internal wave bore in the shelf zone of the sea. *J. Appl. Mech. Tech. Phys.* 2017, 58, 5, 809–818. doi: 10.1134/S0021894417050066
31. *Samchenko A.N.*, *Yaroshchuk I.O.*, *Kosheleva A.V.* Internal gravity waves in the coastal zone of the Sea of Japan according to the natural observations. *Reg. Stud. Mar. Sci.* 2018, 18, 156–160. doi: 10.1016/j.rsma.2018.02.004
32. *Yaroshchuk I.O.*, *Leont'ev A.P.*, *Kosheleva A.V.*, *Pivovarov A.A.*, *Samchenko A.N.*, *Stepanov D.V.*, *Shvyryov A.N.* On intense internal waves in the coastal zone of the Peter the Great Bay (the Sea of Japan). *Russ. Meteorol. Hydrol.* 2016, 41, 629–634. doi: 10.3103/S1068373916090053
33. *Prants S.V.*, *Ponomarev V.I.*, *Budyansky M.V.*, *Uleysky V.Y.*, *Fayman P.A.* Lagrangian analysis of mixing and transport of water masses in the marine bays. *Izv. Atmos. Ocean. Phys.* 2013, 49, 1, 82–96. doi: 10.1134/S0001433813010088
34. *Jiang L.*, *Breaker L.C.*, *Yan X.-H.* Upwelling age: an indicator of local tendency for coastal upwelling. *J. Oceanogr.* 2012, 68, 2, 337–344. doi: 10.1007/s10872–011–0096–2

К статье *Кошелева А.В.*, *Ярощук И.О.*, *Храпченков Ф.Ф.*, *Пивоваров А.А.*, *Самченко А.Н.*, *Швырев А.Н.*, *Коротченко Р.А.* Апвеллинг на узком шельфе Японского моря в 2011 г.
Kosheleva A.V., *Yaroshchuk I.O.*, *Khrapchenkov F.F.*, *Pivovarov A.A.*, *Samchenko A.N.*, *Shvyrev A.N.*, *Korotchenko R.A.* Upwelling on the narrow shelf of the Sea of Japan in 2011

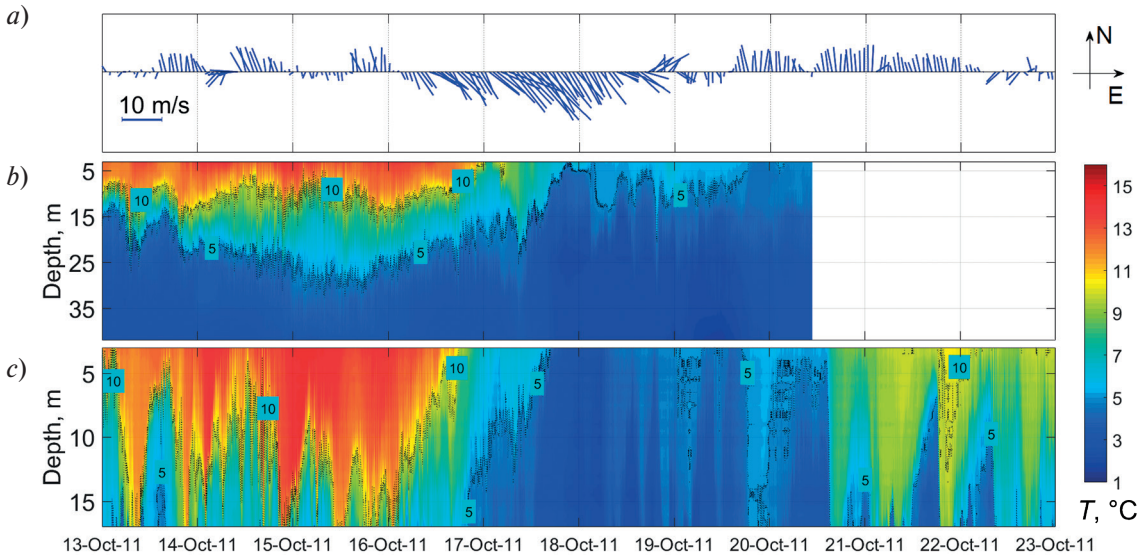

Fig. 2. Wind speed and sea water temperature measurements in October 13–23, 2011: Hourly wind vectors according to the meteorological data from MS "Aanderaa" (*a*) and a time series of water temperature vertical distribution obtained using thermostrings S1 (*b*) and S2 (*c*).

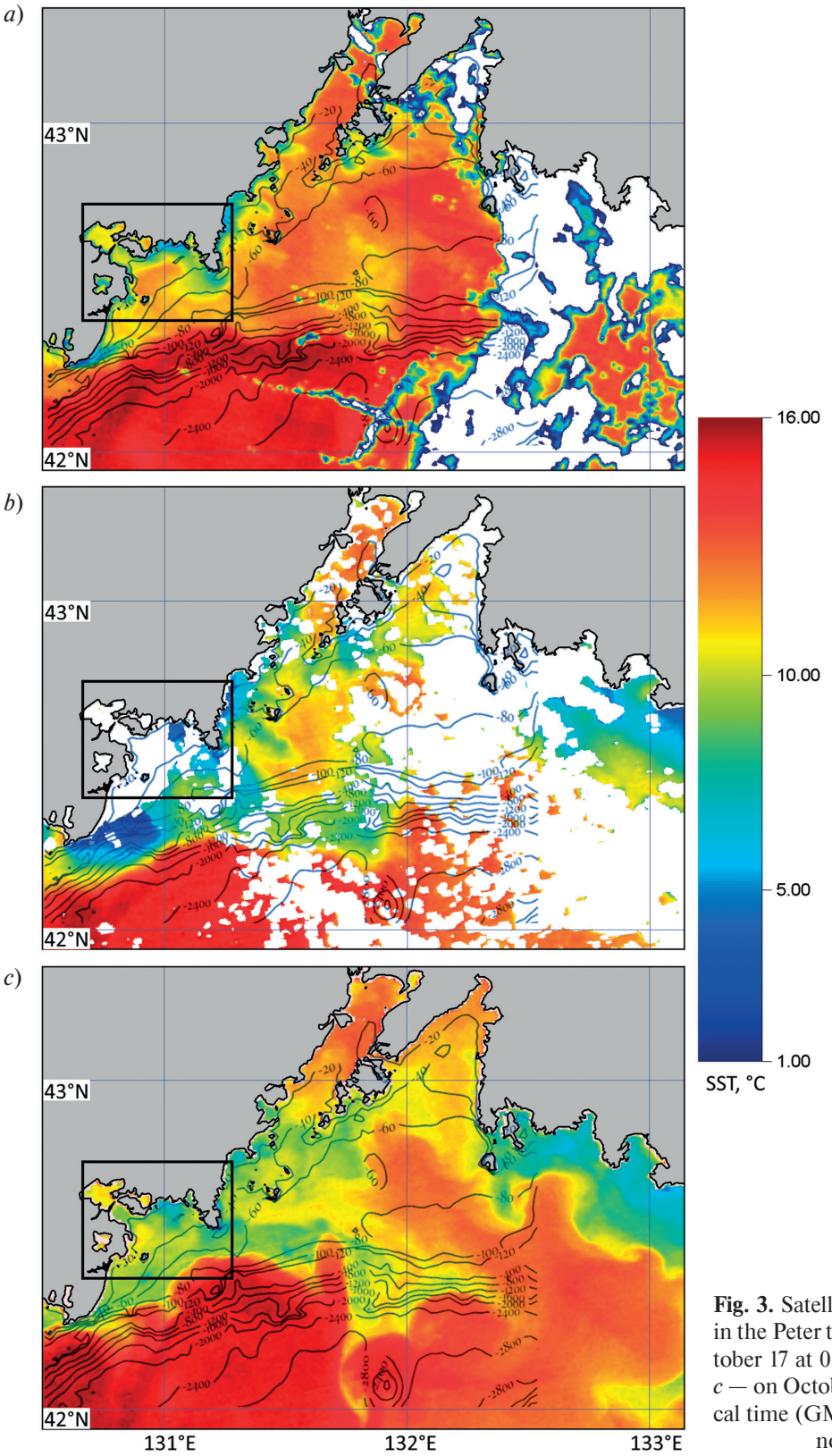

Fig. 3. Satellite images of the SST distribution in the Peter the Great Bay in 2011: *a* — on October 17 at 04:19, *b* — on October 17 at 15:25, *c* — on October 19 at 15:13 according to the local time (GMT+11:00). The simulated area is noted with the rectangle.

К статье *Кошелева А.В.*, *Ярощук И.О.*, *Храпченков Ф.Ф.*, *Пивоваров А.А.*, *Самченко А.Н.*, *Швырев А.Н.*, *Коротченко Р.А.* Апвеллинг на узком шельфе Японского моря в 2011 г.
Kosheleva A.V., *Yaroshchuk I.O.*, *Khrapchenkov F.F.*, *Pivovarov A.A.*, *Samchenko A.N.*, *Shvyrev A.N.*, *Korotchenko R.A.* Upwelling on the narrow shelf of the Sea of Japan in 2011

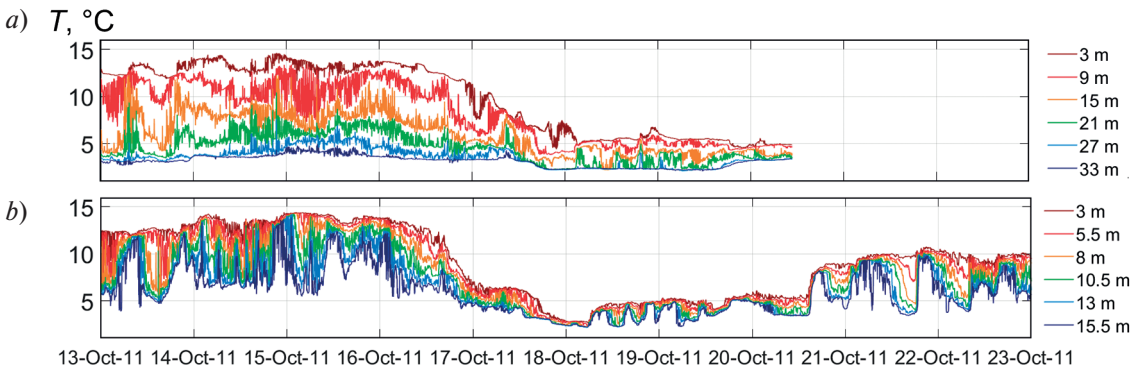

Fig. 4. Time variability of the water temperature according to S1 (*a*) and S2 (*b*) data in the period October 13–23, 2011.

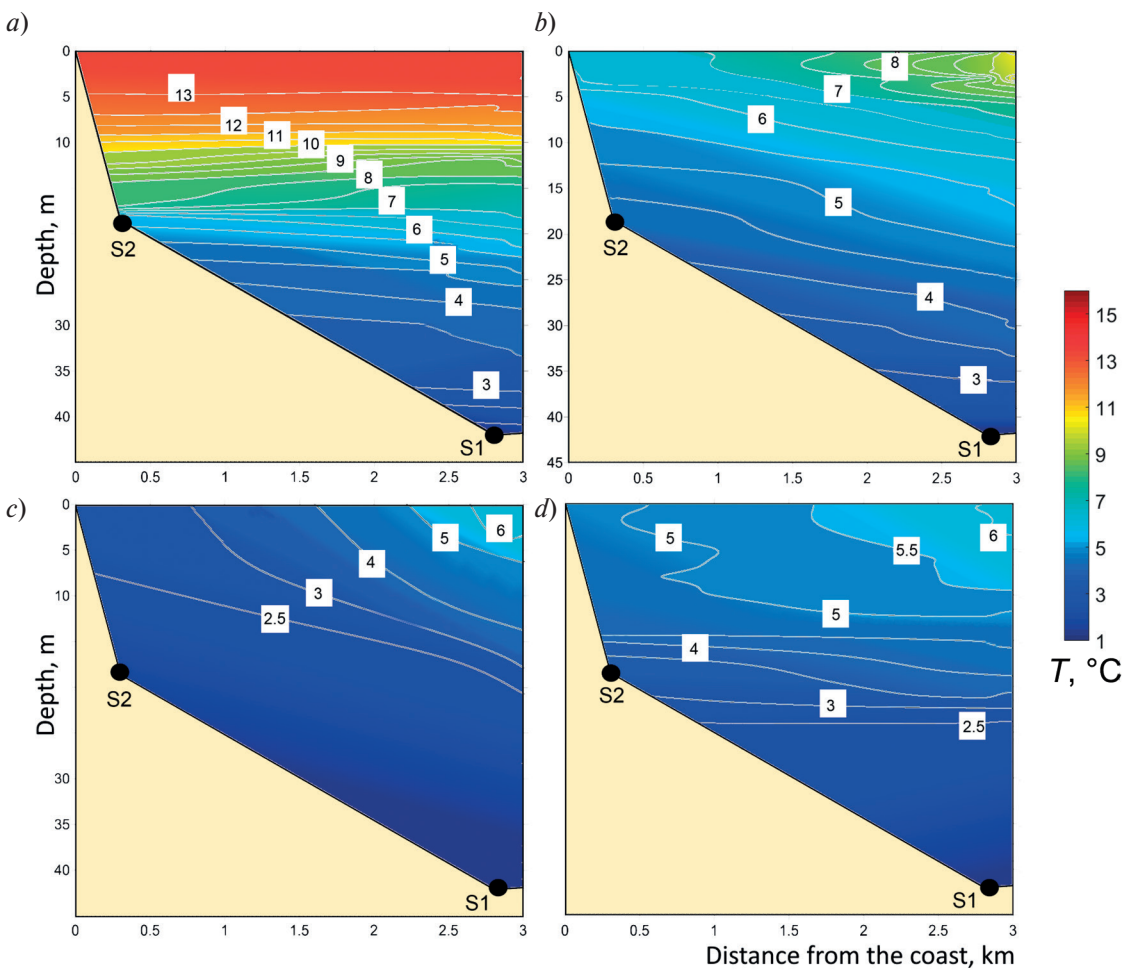

Fig. 5. Water temperature distribution as of October 16 at 06:00 (*a*), 17 at 02:00 (*b*), 18 at 01:50 (*c*) and 18 at 22:00 (*d*), 2011. S1 and S2 are location points of thermostrings.

К статье *Кошелева А.В.*, *Ярощук И.О.*, *Храпченков Ф.Ф.*, *Пивоваров А.А.*, *Самченко А.Н.*, *Швырев А.Н.*, *Коротченко Р.А.* Апвеллинг на узком шельфе Японского моря в 2011 г.
Kosheleva A.V., *Yaroshchuk I.O.*, *Khrapchenkov F.F.*, *Pivovarov A.A.*, *Samchenko A.N.*, *Shvyrev A.N.*, *Korotchenko R.A.* Upwelling on the narrow shelf of the Sea of Japan in 2011

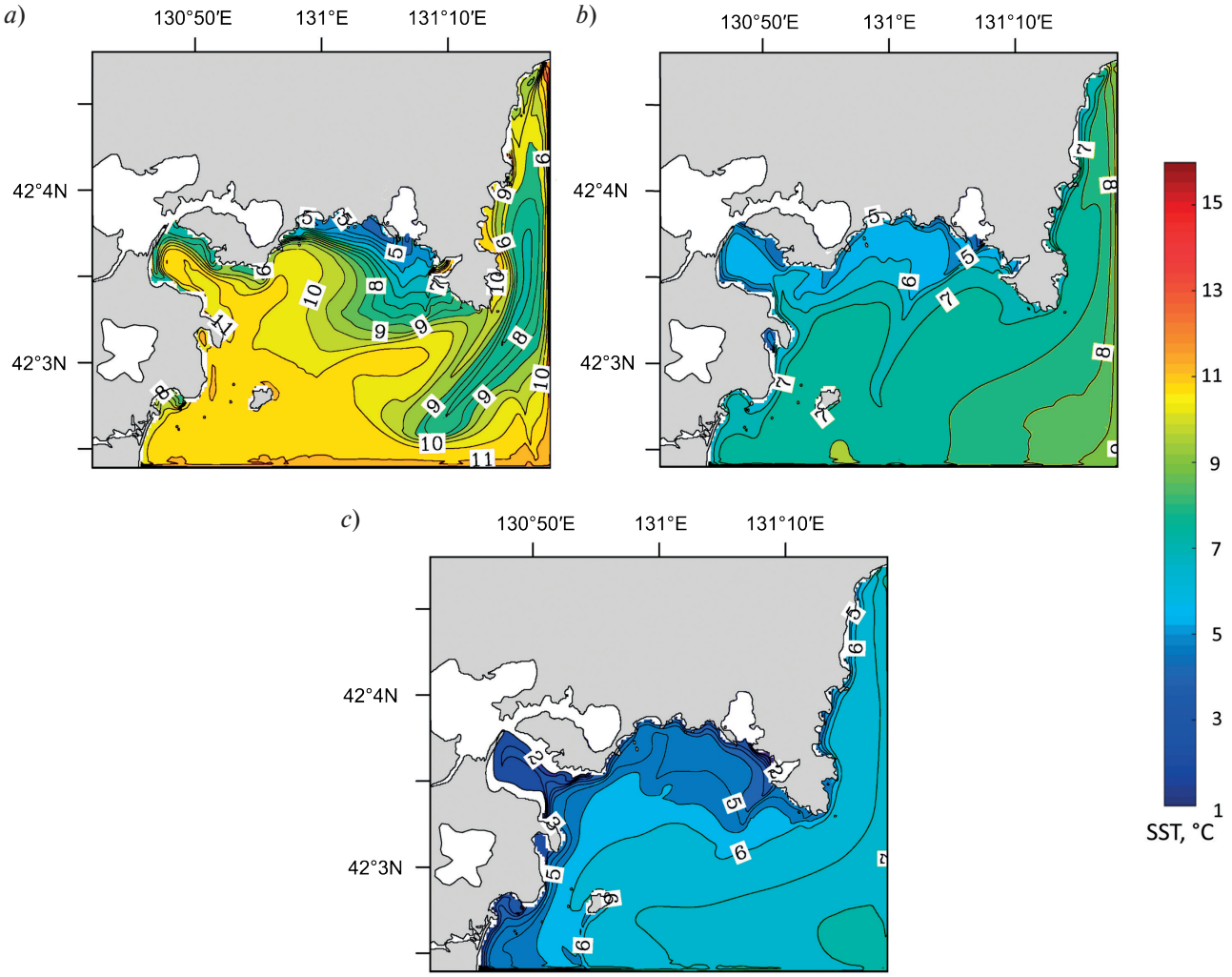

Fig. 10. Simulated surface water temperature in the study area for October 17 at 04:00 (*a*), October 17 at 15:00 (*b*), October 18 at 02:00 (*c*), 2011.

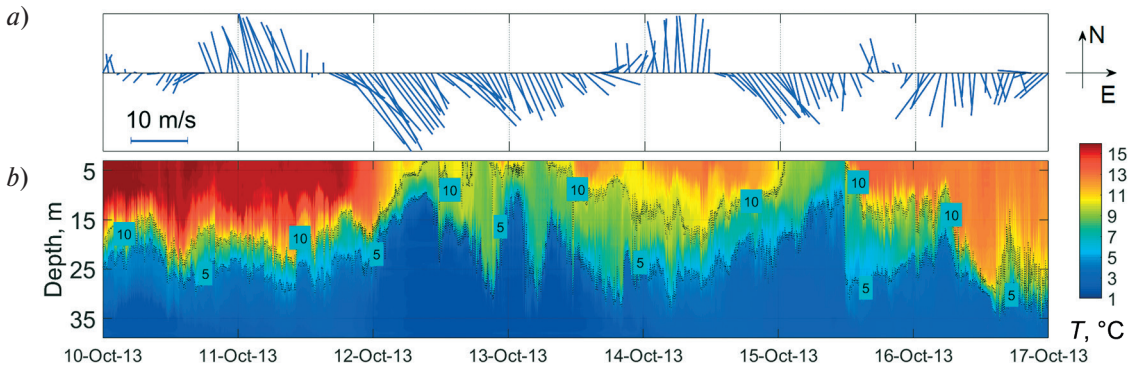

Fig. 11. Wind speed and sea water temperature measurements in October 10–17, 2013: Hourly wind vectors according to the meteorological data from MS “Aanderaa” (*a*) and a time series of water temperature vertical distribution obtained using thermostring S1 (*b*).